Mp*WIP* regulates air pore complex development in the liverwort *Marchantia polymorpha*

Victor AS Jones, Liam Dolan

Department of Plant Sciences, University of Oxford, OX1 3RB, United Kingdom

Summary statement

The Mp*WIP* gene controls the development of the air pore complex – a multicellular structure that increases CO_2 uptake – in the early-diverging land plant *Marchantia polymorpha.*

Keywords

Marchantia polymorpha, air pore complex, WIP protein

ABSTRACT

The colonisation of the land by plants was accompanied by the evolution of complex tissues and multicellular structures comprising different cell types as morphological adaptations to the terrestrial environment. Here we show that the single WIP protein in the early-diverging land plant *Marchantia polymorpha* L. is required for the development of the multicellular gas exchange structure, the air pore complex. This 16-cell barrel-shaped structure surrounds an opening between epidermal cells that facilitates the exchange of gasses between the chamber containing the photosynthetic cells inside the plant and the air outside. Mp*WIP* is expressed in cells of the developing air pore complex and the morphogenesis of the complex is defective in plants with reduced Mp*WIP* function. The role of WIP proteins in the control of different multicellular structures in *M. polymorpha* and the flowering plant *Arabidopsis thaliana* suggests that these proteins controlled the development of multicellular structures in the common ancestor of land plants. We hypothesise that *WIP* genes were subsequently co-opted in the control of morphogenesis of novel multicellular structures that evolved during the diversification of land plants.

INTRODUCTION

Morphological diversity increased dramatically after plants colonised the land some time before 460 million years ago (Kenrick and Crane, 1997). The evolution of unicellular and multicellular structures with specialised functions in the outermost cell layer – the epidermis – provided plants with the means to increase the surface area over which CO_2 uptake from the atmosphere occurred, and to extract water and inorganic nutrients from the early soil. Some specialized epidermal structures are present in all extant lineages of land plants. For example, tip-growing rhizoids and root hairs emerge from the epidermis to provide anchorage and take up water and nutrients from the soil (Jones and Dolan 2012). The phylogenetic distribution of others is more restricted; stomata, valves in the epidermis consisting of two specialized guard cells that open and close to regulate gas exchange, develop in all land plant lineages except the early-diverging Marchantiophyta (liverworts). In one group of liverworts, the Marchantiidae, the evolution of complex tissues has been accompanied by an independent evolution of a multicellular epidermal structure that facilitates gas exchange, the air pore complex (Crandall-Stotler et al., 2009). We report here that the zinc finger protein MpWIP is necessary for the morphogenesis of the air pore complex in the epidermis of *Marchantia polymorpha*.

RESULTS AND DISCUSSION

A gain-of-function mutation in Mp*WIP* causes defective development of the dorsal epidermis

To identify genetic mechanisms controlling the development of specialised morphological structures that operated in the earliest land plants we screened for mutants with defects in the development of epidermal structures in the liverwort *Marchantia polymorpha*, a member of one of the earliest-diverging groups of land plants. Multicellular air pore complexes, gemma cups and gemmae develop on the dorsal epidermis of *M. polymorpha* (Fig. 1 A,C) while unicellular rhizoids and multicellular membranous outgrowths (scales) develop on the ventral epidermis (Fig. 1 B,D). In a screen of T-DNA insertion mutants (Honkanen et al., 2016) we isolated a mutant, *vj7*, that develops rhizoids from the epidermal cells of the mature dorsal epidermis (3.76 rhizoids/mm^2, n=5); rhizoids do not develop on the dorsal epidermis

of the wild type (Fig. 1 E,F). The dorsal rhizoid phenotype of mutant *vj7* results from a single mutation that is tightly linked to a T-DNA insertion 764 bp upstream of the transcriptional start site of a gene (Supplemental Data 1) encoding a member of the WIP zinc finger protein family, MpWIP (GenBank: KX645870) (Fig. 1 G, Figs S1,S2).

We hypothesised that the T-DNA insertion in *vj7* would impact the transcription of the Mp*WIP* gene 3' from the T-DNA right border. To quantify the effects of this insertion on Mp*WIP* expression, we measured the steady-state levels of Mp*WIP* transcript in the wild type and mutant *vj7*. Mp*WIP* transcript level was almost four times higher in *vj7* than in the wild type Tak-2 (Fig. 1 H), consistent with the hypothesis that *vj7* is a gain-of-function Mp*wip* mutant. To independently verify that Mp*WIP* gain-of-function induces the development of rhizoids on the dorsal surface of *M. polymorpha*, we expressed Mp*WIP* under the control of the constitutively-active Os*ACTIN* promoter ($_{pro}$ Os*ACT:*Mp*WIP*) (Breuninger et al., 2016), and isolated a line in which the level of Mp*WIP* transcript is twice that seen in the wild type (Fig. 1 H). Plants of this line developed ectopic rhizoids on the dorsal surface, as observed in *vj7* but not the wild type Tak-2 (Fig.1 I). This is consistent with the hypothesis that a gain of Mp*WIP* function causes the development of ectopic rhizoids in mutant *vj7*. We conclude that *vj7* is a gain-of-function mutant of Mp*WIP* and designated it Mp*wip-1*^{GOF}.

The Mp*WIP* promoter is active in developing air pores

To investigate where the Mp*WIP* promoter is active in the wild type we expressed *3xYFP-NLS* under the control of a 4.7 kb fragment of genomic DNA upstream of the CDS of Mp*WIP* ($_{pro}$Mp*WIP*:*YFP-NLS*). In plants transformed with $_{pro}$Mp*WIP*:*YFP-NLS* fluorescent protein was detected in cells in the apical region of both the ventral and dorsal sides of the thallus (Fig. 2 A). The activity of the promoter in the ventral apical region, where rhizoids initiate, is consistent with a possible role for Mp*WIP* in promoting rhizoid development. On the dorsal side of the thallus the Mp*WIP* promoter was most active in cells of developing air pore complexes (Fig. 2 A), with lower activity in the surrounding epidermal cells. Air pores initiate as schizogenous openings that form in the epidermis at points where four cells meet (Apostolakos and Galatis, 1985a). The four cells surrounding each opening divide periclinally and

differentiate to form the multiple tiers of the barrel-shaped air pore (Fig. 2 B) (Apostolakos and Galatis, 1985a). Air chambers form below the air pores and consist of schizogenous intercellular cavities in which filaments of photosynthetic cells develop (Apostolakos and Galatis, 1985b; Ishizaki et al., 2013; Mirbel, 1835). Low levels of $_{pro}$Mp*WIP* activity were detected in all cells near the apex before air pore differentiation is visible, and this activity increased in the dividing cells of the developing air pore complex. The strong promoter activity in cells of the air pore complexes compared to surrounding cells is first apparent at the four-cell stage, when the cells surrounding the schizogenous opening first enlarge relative to the surrounding epidermal cells (Fig. 2 A,B). Strong expression continues during the periclinal divisions that generate the tiered 16-cell air pore complex (Fig. 2 A,B). The activity of the Mp*WIP* promoter during the formation of air pore complexes suggested that MpWIP could be involved in their development.

MpWIP is required for air pore development

To determine if MpWIP is required for rhizoid or air pore complex development we generated plants with decreased Mp*WIP* function. We expressed two different artificial microRNAs based on Mp*miR160* (Flores-Sandoval et al., 2016) that target either the 3' UTR (*amiR*-Mp*WIP-3' UTR*$^{Mp miR160}$) or CDS (*amiR*-Mp*WIP-CDS*$^{Mp miR160}$) of Mp*WIP* under the control of $_{pro}$Os*ACT*. Steady-state levels of Mp*WIP* transcript are reduced to approximately half wild type levels in plants transformed with $_{pro}$Os*ACT:amiR*-Mp*WIP-3' UTR*$^{Mp miR160}$ or $_{pro}$Os*ACT:amiR*-Mp*WIP-CDS*$^{Mp miR160}$ (Fig. 3 A,B). The formation of the air chambers is delayed or abolished in the Mp*WIP* knockdown lines, and consequently the reticulated pattern of dark green air chambers characteristic of the wild type is absent (Fig. 3 A). Furthermore, the regular 16-cell structure of the wild-type air pore complex does not develop (Fig. 3 C). Air pore development begins with the formation of schizogenous openings at the point where four cells meet, exactly as it does in the wild type (Fig S 4 A). However, the periclinal divisions that form the tiers of the air pore complex in wild type mostly fail to occur in the knockdown lines. Instead cells divide anticlinally, forming a single tier of more than four cells surrounding the pore (Fig S 4 B). This indicates that reducing the level of Mp*WIP* transcript disrupts air pore morphogenesis after the four cell

stage, consistent with a role of Mp*WIP* in air pore complex and air chamber development suggested by the activity of $_{pro}$Mp*WIP* during air pore development (Fig. 2 A). We were unable to quantify rhizoid density, but rhizoid development was indistinguishable from the wild type. Together these data indicate that Mp*WIP* activity is required for the differentiation of air pore complexes, but do not provide evidence that it is necessary for rhizoid development.

MpWIP may act as a transcriptional repressor

At least one WIP protein, AtNO TRANSMITTING TRACT (AtNTT), binds DNA (Marsch-Martínez et al., 2014). To determine if MpWIP promotes rhizoid identity and air pore complex development through transcriptional activation or repression, we expressed chimeric dominant repressor and activator versions of MpWIP separately in transgenic plants. To generate the dominant repressor, we fused an SRDX repressive domain (Hiratsu et al., 2003) to the C-terminus of MpWIP, and to make the dominant activator we fused a VP16 activator domain to the C-terminus (Liu and Stewart, 2016; Sadowski et al., 1988; Wilde et al., 1994). Each of these fusion proteins was expressed using the constitutive CaMV 35S promoter ($_{pro}$*35S:*Mp*WIP-SRDX* and $_{pro}$*35S:*Mp*WIP-VP16*). If MpWIP promotes rhizoid and air pore differentiation via transcriptional repression, we predicted that (i) supernumerary rhizoids would develop on plants that express Mp*WIP-SRDX*, as observed in plants overexpressing Mp*WIP* function (Fig. 1 E,F,H,I) and (ii) plants expressing Mp*WIP-VP16* would develop a defective air pore phenotype similar to that caused by a loss of Mp*WIP* function, in $_{pro}$Os*ACT:amiR*-Mp*WIP-3' UTR*$^{Mp miR160}$ and $_{pro}$Os*ACT:amiR*-Mp*WIP-CDS*$^{Mp miR160}$ lines (Fig. 3 A,B,C).

Plants transformed with $_{pro}$*35S:*Mp*WIP:SRDX* that expressed the transgene (Fig. 4 A) developed a dense growth of ectopic rhizoids on the dorsal surface of the thallus, while air pore development was similar to wild type (Fig. 4 C). This is similar to the phenotype of the Mp*wip*^{GOF} mutant and $_{pro}$*OsACT:*Mp*WIP* line (Fig.1 E,F,I). The expression of a repressive form of Mp*WIP* therefore results in the development of plants that are morphologically similar to plants that overexpress native Mp*WIP*, consistent with the hypothesis that MpWIP is a transcriptional repressor. Plants that express the Mp*WIP-VP16* transgene (Fig. 4 C) developed phenotypic defects comparable to those in lines with reduced Mp*WIP* function, where air chamber (Fig. 4 D, Fig. 3 A) and air pore complex development are defective (Fig. 4 E, Fig. 3 C). This suggests that expression of a form of MpWIP that promotes transcriptional activation has developmental effects similar to a loss of Mp*WIP* function. Therefore, the phenotypes of both Mp*WIP:SRDX* and Mp*WIP:VP16* lines are consistent with the

hypothesis that MpWIP promotes the morphogenesis of air pore complexes through transcriptional repression.

We conclude that Mp*WIP* is necessary for the morphogenesis of the multicellular air pore complex in the dorsal epidermis of *M. polymorpha*; air pore morphology is defective in plants with reduced WIP activity. *WIP* genes are also required for the development of various multicellular structures in the angiosperm *A. thaliana.* For example, AtNTT is a WIP protein required for the development of the replum, a structure that facilitates dehiscence and seed dispersal from *A. thaliana* fruits (Marsch-Martínez et al., 2014) – cell number is reduced in the repla of At*ntt* mutant fruits compared to wild type. Roots do not form in At*ntt* At*wip4* At*wip5* triple mutants, demonstrating a requirement for these three related WIP proteins in the development of the distal stem cells of the root during embryogenesis (Crawford et al., 2015). Incomplete veins form in At*defectively organised tributaries5* (At*dot5*) mutants, indicating the requirement of the WIP protein AtDOT5 in leaf vein development (Petricka et al., 2008). The demonstration that WIP proteins control the development of different multicellular structures in both early-diverging land plants and angiosperms (the latest-derived land plants) leads us to propose that WIP proteins controlled the development of multicellular structures in the common ancestor of *M. polymorpha* and *A. thaliana*, a close relative of the earliest land plants. We hypothesise that the subsequent duplication of *WIP* genes and neofunctionalisation of WIP proteins promoted the development of novel multicellular structures that evolved as the morphologies of land plants diversified.

MATERIALS AND METHODS

See Supplemental Information for primer sequences and plasmid construction.

Plant material and growth

Tak-1 male and Tak-2 female wild type accessions (Ishizaki et al., 2008) were used in this study. Mutant *vj7* was isolated in a mutant screen of spores from a cross between Tak-1 and Tak-2 transformed with the T-DNA vector pCambia1300 (Honkanen et al., 2016). Plants were grown as previously described (Honkanen et al., 2016).

Microscopy

Images were obtained using a Leica M165FC stereomicroscope, Leica M series Plan APO 1.0x objective and Leica DFC310 FX camera. For confocal microscopy plants were stained with 15 µM propidium iodide for 15 minutes, then submerged in water. Images were acquired with a Leica SP5 confocal microscope using a Leica HCX APO 40x/0.80 W U-V-I dipping lens with sequential scans. YFP fluorescence was detected using excitation at 514 nm with an argon laser and emission was measured between 524 and 568 nm using an Acousto-Optic Tunable Filter. PI was excited at 543 nm using a helium-neon laser and emission measured between 568 and 659 nm. Images were processed using FIJI to create brightest-point 3d projections (Schindelin et al., 2012).

For scanning electron microscopy samples were fixed in dry methanol, critical point dried using a Tousimis Autosamdri-815, mounted on aluminium stubs and coated with a gold/palladium mixture using a Quorum Technologies SC7640 sputter coater. Samples were imaged immediately with a JEOL JSM-5510 SEM.

Molecular analysis of mutant *vj7* and gene expression analysis

Genomic sequences flanking T-DNA insertions were isolated by TAIL-PCR as previously described (Proust et al., 2016). Genes near the site of the insertion linked to the mutant phenotype in line *vj7* were identified using the blastn algorithm, with 5 kb of genomic sequence 3’ and 5’ to the insertion site as the template, to query an *M. polymorpha* transcriptome (Honkanen et al., 2016).RNA extraction, cDNA synthesis and quantitative PCRs (qPCRs) were carried out as previously described

(Breuninger et al., 2016). Mp*ACT* and Mp*APT* were used as reference genes (Saint-Marcoux et al., 2015).

ACKNOWLEDGEMENTS

This research was funded by European Research Council Advanced Grant (Project number 25028) EVO-500 to LD. VASJ was funded by a Newton Abraham Studentship. We are grateful to Alexander J. Hetherington, Clément Champion, Bruno Catarino, Anna Thamm, Dr Holger Breuninger, Dr Clémence Bonnot, and Dr Ana Milhinhos for discussions and comments on the manuscript.

AUTHOR CONTRIBUTIONS

Conceptualization, LD; Methodology, VASJ, LD; Investigation, VASJ; Writing – Original Draft, VASJ, LD; Writing – Review and Editing, VASJ, LD; Supervision, LD; Funding Acquisition, LD

REFERENCES

Apostolakos, P. and Galatis, B. (1985a). Studies on the development of the air pores and air chambers of *Marchantia paleacea*. IV. Cell plate arrangement in initial aperture cells. *Protoplasma* **128**, 136–146.

Apostolakos, P. and Galatis, B. (1985b). Studies on the development of the air pores and air chambers of *Marchantia paleacea* III . Microtubule organization in preprophase-prophase initial aperture cells - formation of incomplete preprophase microtubule bands. *Protoplasma* **128**, 120–135.

Breuninger, H., Thamm, A., Streubel, S., Sakayama, H., Nishiyama, T. and Dolan, L. (2016). Diversification of a bHLH transcription factor family in streptophytes led to the evolution of antagonistically acting genes controlling root hair growth. *Curr. Biol.* **26**, 920–934.

Crandall-Stotler, B., Stotler, R. E. and Long, D. G. (2009). Phylogeny and classification of the Marchantiophyta. *Edinburgh J. Bot.* **66**, 155.

Crawford, B. C. W., Sewell, J., Golembeski, G., Roshan, C., Long, J. A. and Yanofsky, M. F. (2015). Genetic control of distal stem cell fate within root and embryonic meristems. *Science (80-.).* **347**, 655–59.

Flores-Sandoval, E., Dierschke, T., Fisher, T. J. and Bowman, J. L. (2016). Efficient and inducible use of artificial microRNAs in *Marchantia polymorpha*. *Plant Cell Physiol.* **57**, 281–90.

Hiratsu, K., Matsui, K., Koyama, T. and Ohme-Takagi, M. (2003). Dominant repression of target genes by chimeric repressors that include the EAR motif, a repression domain, in *Arabidopsis*. *Plant J.* **34**, 733–739.

Honkanen, S., Jones, V. A. S., Morieri, G., Champion, C., Hetherington, A. J., Kelly, S., Proust, H., Saint-Marcoux, D., Prescott, H. and Dolan, L. (2016). The mechanism forming the cell surface of tip-growing rooting cells is conserved among land plants. *Curr. Biol.* **26**, 3238–3244.

Ishizaki, K., Chiyoda, S., Yamato, K. T. and Kohchi, T. (2008). Agrobacterium-mediated transformation of the haploid liverwort *Marchantia polymorpha* L., an

emerging model for plant biology. *Plant Cell Physiol.* **49**, 1084–91.

Ishizaki, K., Mizutani, M., Shimamura, M., Masuda, A., Nishihama, R. and Kohchi, T. (2013). Essential role of the E3 ubiquitin ligase NOPPERABO1 in schizogenous intercellular space formation in the liverwort *Marchantia polymorpha*. *Plant Cell* **25**, 4075–84.

Jones, V. A. S. and Dolan, L. (2012). The evolution of root hairs and rhizoids. *Ann. Bot.* **110**, 205–12.

Kenrick, P. R. and Crane, P. R. (1997). *The origin and early diversification of land plants: a cladistic study*. 1st ed. Washington, D. C.: Smithsonian Institution Press.

Liu, W. and Stewart, C. N. (2016). Plant synthetic promoters and transcription factors. *Curr. Opin. Biotechnol.* **37**, 36–44.

Marsch-Martínez, N., Zúñiga-Mayo, V. M., Herrera-Ubaldo, H., F Ouwerkerk, P. B., Pablo-Villa, J., Lozano-Sotomayor, P., Greco, R., Ballester, P., Balanzá, V., H Kuijt, S. J., et al. (2014). The NTT transcription factor promotes replum development in Arabidopsis fruits. *Plant J.* 1–13.

Mirbel, M. (1835). Recherches anatomiques et physiologiques sur le Marchantia polymorpha, pour servir a l'histoire du tissue cellulaire, de l'épiderme et des stomates. *Mém. l'Acad. R. des Sci. l'Inst. Fr.* **Tome XIII**, 337–373.

Petricka, J. J., Clay, N. K. and Nelson, T. M. (2008). Vein patterning screens and the defectively organized tributaries mutants in *Arabidopsis thaliana*. *Plant J.* **56**, 251–63.

Proust, H., Honkanen, S., Jones, V. A. S., Morieri, G., Prescott, H., Kelly, S., Ishizaki, K., Kohchi, T. and Dolan, L. (2016). *RSL* class I genes controlled the development of epidermal structures in the common ancestor of land plants. *Curr. Biol.* **26**, 93–99.

Sadowski, I., Ma, J., Triezenberg, S. and Ptashne, M. (1988). GAL4-VP16 is an unusually potent transcriptional activator. *Nature* **335**, 563–564.

Saint-Marcoux, D., Proust, H., Dolan, L. and Langdale, J. A. (2015). Identification

of reference genes for real-time quantitative PCR experiments in the liverwort *Marchantia polymorpha*. *PLoS One* **10**, e0118678.

Schindelin, J., Arganda-Carreras, I., Frise, E., Kaynig, V., Longair, M., Pietzsch, T., Preibisch, S., Rueden, C., Saalfeld, S., Schmid, B., et al. (2012). Fiji: an open-source platform for biological-image analysis. *Nat. Methods* **9**, 676–682.

Wilde, R. J., Cooke, S. E., Brammar, W. J. and Schuch, W. (1994). Control of gene expression in plant cells using a 434:VP16 chimeric protein. *Plant Mol. Biol.* **24**, 381–8.

Figures

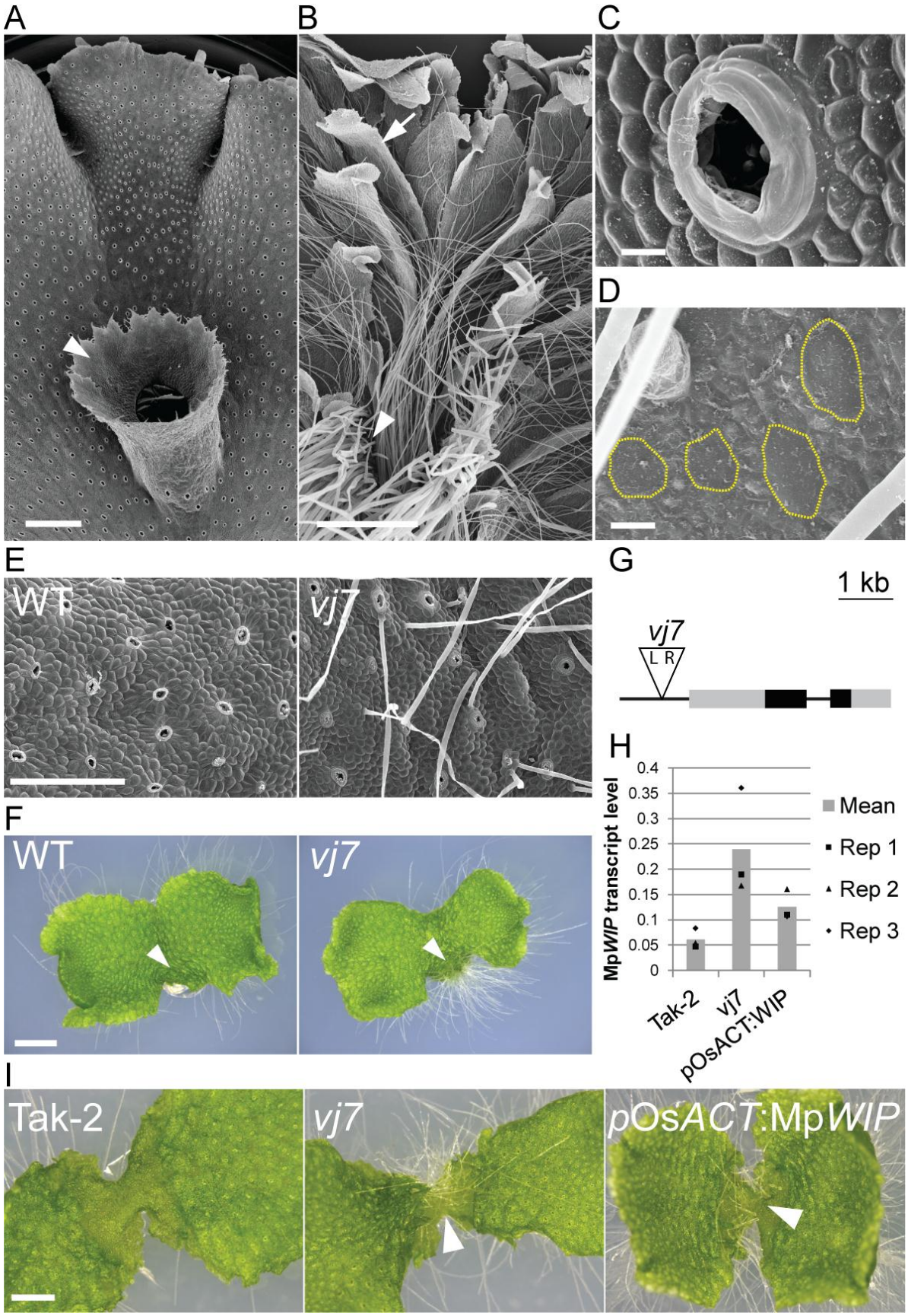

Figure 1 A gain-of-function mutant of Mp*WIP* develops ectopic rhizoids on the dorsal surface. A) Air pores and gemma cups (arrowhead) are produced on the dorsal thallus surface. Scale 1 mm, apex at top. B) Scales (arrow) and rhizoids (arrowhead) are produced on the ventral thallus surface. Scale 1 mm, apex at top. C) Detail of air pore complex. Scale 20 µm. D) Detail of ventral rhizoid patch. Cells that will develop into rhizoids (yellow outlines) are separated by non-rhizoid cells. Scale 20 µm. E) Rhizoids develop on the dorsal surface of older parts of the mature thallus of *vj7* but not wild type. 43 d, scale 500 µm. F) Sporelings of *vj7* produce rhizoids on the oldest part of the dorsal thallus surface (arrowhead). This region of wild type sporelings lacks rhizoids. 28 d, scale 2 mm. G) The T-DNA insertion that cosegregates with the mutant phenotype in *vj7* is located 5' to Mp*WIP*. Boxes represent exons; black are CDS, grey are untranslated regions. H) Mp*WIP* transcript levels are greater in mutant *vj7* and $_{pro}$ Os*ACT:*Mp*WIP* than wild type Tak-2. 14 d gemmalings. I) Expression of Mp*WIP* driven by the constitutive promoter $_{pro}$Os*ACT* causes the development of ectopic rhizoids (arrowheads), as in mutant *vj7*. 10 d gemmalings, scale 1 mm.

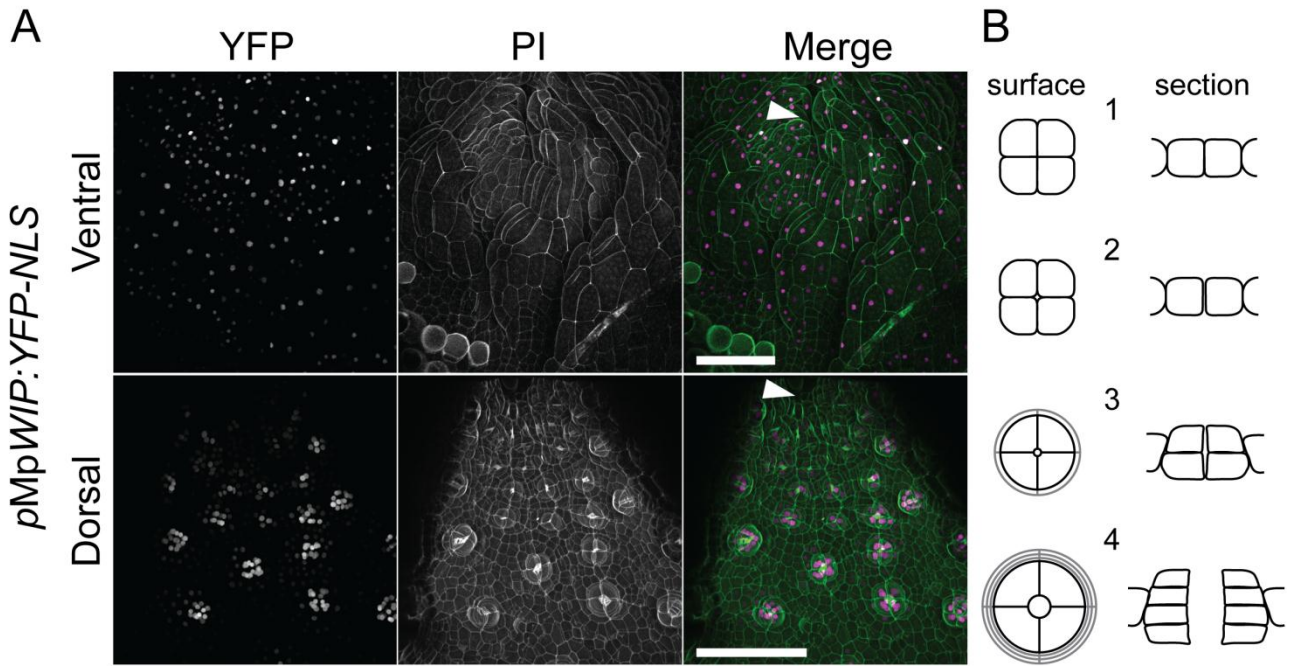

Figure 2 The Mp*WIP* promoter is active in the ventral apical region and in developing air pores. A) Apical region of the ventral (top row) and dorsal (bottom row) surface of the thallus of $_{pro}$Mp*WIP:3xYFP-NLS*. 9 d gemmaling, scale 100 µm, apex at arrowhead. B) Schematic of the stages of air pore development. A schizogenous opening develops at the point where four epidermal cells meet (stages 1 and 2). Periclinal divisions then give rise to a stack of rings, each consisting of four cells (stages 3 and 4). Surface view (left) and cross section (right). After (Apostolakos and Galatis, 1985a).

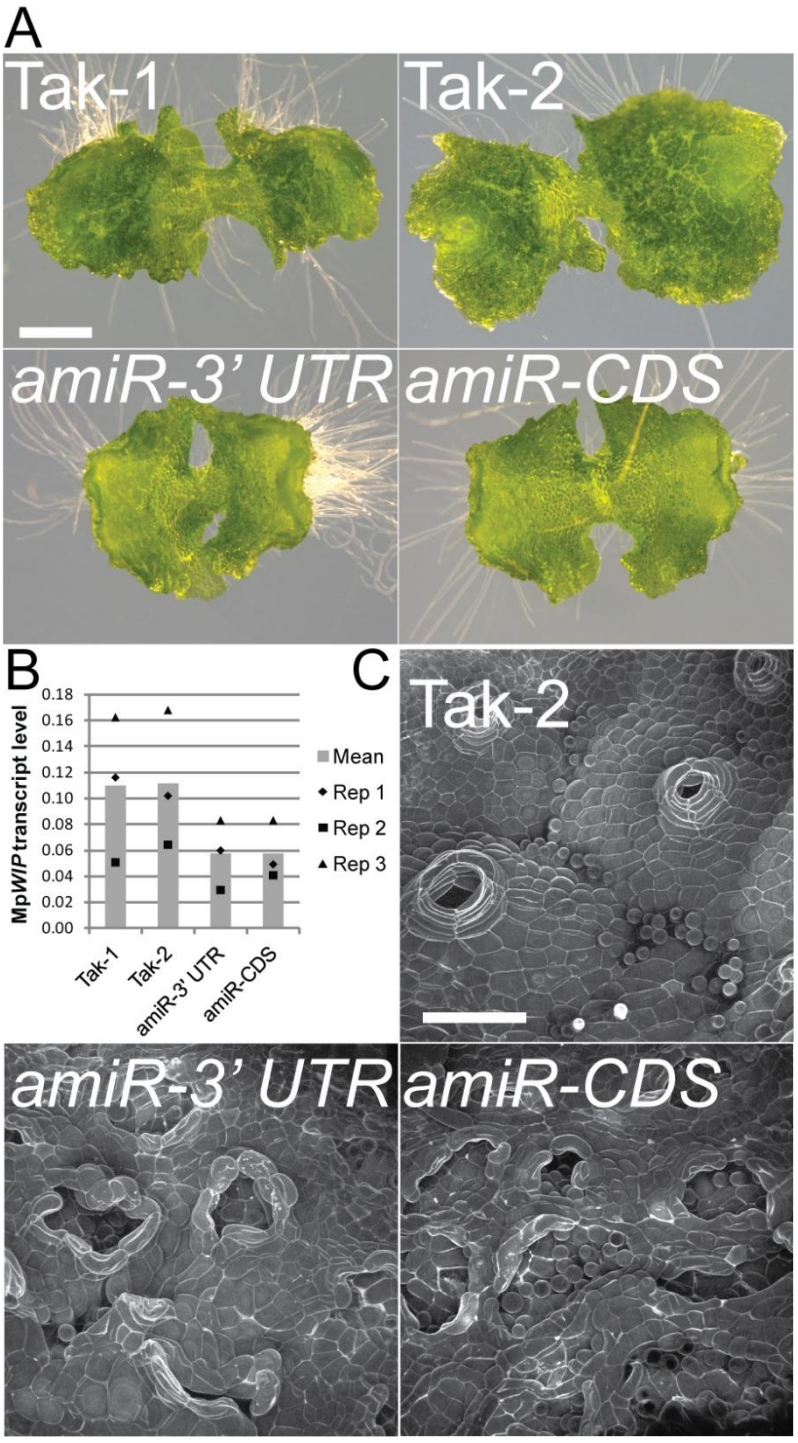

Figure 3 Reduced Mp*WIP* expression causes defects in air pore development. A) The dark green air chambers seen in the wild type (Tak-1, Tak-2) do not develop in plants transformed with $_{pro}$Os*ACT:amiR*-Mp*WIP-3' UTR*$^{Mp miR160}$ or $_{pro}$Os*ACT:amiR*-Mp*WIP-CDS*$^{Mp miR160}$.10 d gemmalings, scale 1 mm. B) Mp*WIP* transcript levels are reduced in lines transformed with $_{pro}$Os*ACT:amiR*-Mp*WIP-3'*

UTR$^{\text{Mp}miR160}$ or $_{pro}$Os*ACT:amiR*-Mp*WIP-CDS*$^{\text{Mp}miR160}$. 10 d gemmalings. C) Plants with reduced Mp*WIP* transcript levels develop air pores with defective morphology, lacking the regular 16-cell air pore complex structure that develops in the wild type (Tak-2). CSLM, PI stained, 9 d gemmalings, scale 100 µm.

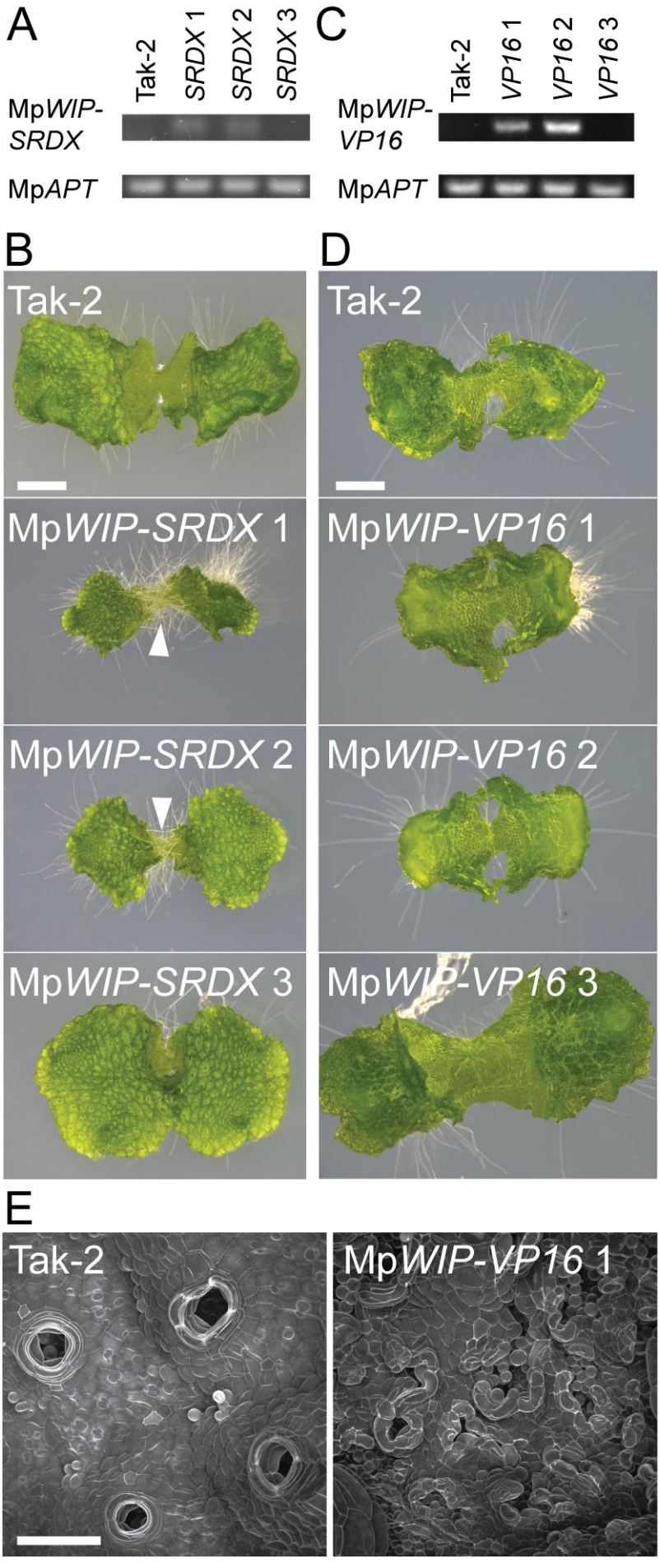

Figure 4 Expression of the dominant repressor Mp*WIP-SRDX* or the dominant activator Mp*WIP-VP16* causes the development of ectopic rhizoids or defective air pores, respectively. A) Mp*WIP:SRDX* transcript is detected in lines $_{pro}$*35S:*Mp*WIP:SRDX* 1 and 2 but not $_{pro}$*35S:*Mp*WIP-SRDX* 3 or Tak-2. 12 d gemmalings. B) Mp*WIP-VP16* transcript is detected in lines $_{pro}$*35S:*Mp*WIP-VP16* 1 and 2 but not $_{pro}$*35S:*Mp*WIP-VP16* 3 or Tak-2. 10 d gemmalings. C) The lines that express Mp*WIP-SRDX* ($_{pro}$*35S:*Mp*WIP-SRDX* 1 and 2) develop ectopic rhizoids on the dorsal surface (arrowheads). 12 d gemmalings, scale 2 mm. D) Air chamber development is defective in lines that express Mp*WIP-VP16* ($_{pro}$*35S:*Mp*WIP-VP16* 1 and 2). 10 d gemmalings, scale 1mm. E) Air pore complex morphology is aberrant in lines that express Mp*WIP-VP16*. CSLM, PI stained, 10 d gemmalings, scale 100 µm.

Supplementary Information for Jones and Dolan

Mp*WIP* regulates air pore complex development in the liverwort *Marchantia polymorpha*

Supplementary Data 1. Genetic analysis of mutant *vj7*

We previously reported that gain of function mutations in Mp*RSL1* cause the development of rhizoids on the dorsal surface (Proust et al., 2016). To rule out the possibility that a mutation in the Mp*RSL1* gene in the *vj7* background was responsible for the development of ectopic rhizoids we crossed *vj7* to two Mp*rsl1*^{GOF} mutants, Mp*rsl1*^{GOF6} (*vj4*) and Mp*rsl1*^{GOF7} (*vj5*). In the F1 generation resulting from the cross between *Mprsl1*^{GOF6} and *vj7,* 64 of 297 plants (22 %) were wild type for rhizoid development and 233 (78%) developed dorsal rhizoids. In the F1 generation of the cross between Mp*rsl1*^{GOF7} and *vj7* 52 of 186 plants (28%) were wild type and 134 were mutant (72%). The presence of plants with a wild type phenotype among the progeny in the F1 generation indicates that the phenotypic defects in *vj7* and Mp*rsl1* are due to mutations of different genes and are therefore not allelic.

To establish whether the ectopic rhizoid trait of mutant *vj7* is controlled by a single Mendelian locus we determined its inheritance. We crossed the mutant to the wild type line Tak-1 and scored the phenotypes of the next generation. Because the phenotype is expressed in the haploid stage, we expected that if the mutant phenotype was caused by a single mutation we would observe a 1:1 ratio of mutant to wild type in the F1 generation. Of 293 F1 plants scored, 131 expressed the mutant phenotype and 162 expressed the wild type phenotype (segregation ratio 1:1.24, χ^2 p=0.07). Having demonstrated that the dorsal rhizoid phenotype of the *vj7* line is controlled by a single genetic locus we set out to determine if it was caused by a T-DNA insertion. The population from which mutant *vj7* was selected was generated by insertional mutagenesis using a T-DNA that confers resistance to hygromycin. If the mutant phenotype always cosegregates with hygromycin resistance, indicating genetic linkage, the insertion is likely to be responsible for the defective phenotype of the mutant. To determine if the mutation causing the development of ectopic rhizoids is linked to the T-DNA we scored hygromicin resistance in the F1 progeny. 100% of the plants that developed dorsal rhizoids were hygromycin resistant, indicating that the mutant phenotype cosegregates with hygromycin resistance. However, 101 (62%) of the wild type phenotype plants were also resistant to hygromycin, indicating that more than one insertion was segregating in the F1 population.

To identify the T-DNA insertion that cosegregates with the mutant phenotype of *vj7* we used TAIL-PCR as previously described (Proust et al., 2016) to find the genomic locations of two T-DNA insertions in *vj7.* We determined the genotype for these insertions of 106 hygromycin-resistant individuals resulting from the cross between *vj7* and the wild type Tak-1, 72 with the mutant phenotype and 34 with the wild type phenotype. One of the insertions (Fig. 1 G, main text) was found in all of

the dorsal rhizoid mutants but in none of the wild type plants, indicating that this insertion is linked to the mutant phenotype. The second insertion was found in all 34 progeny with wild type phenotype and 29 of the 72 of the mutant phenotype progeny (40%), indicating that the second T-DNA is not linked to the mutant phenotype. Taken together these data indicate that the dorsal rhizoid phenotype in the *vj7* line results from a single mutation that is closely linked to the T-DNA insertion shown in Fig. 1 G (main text).

Figure S1

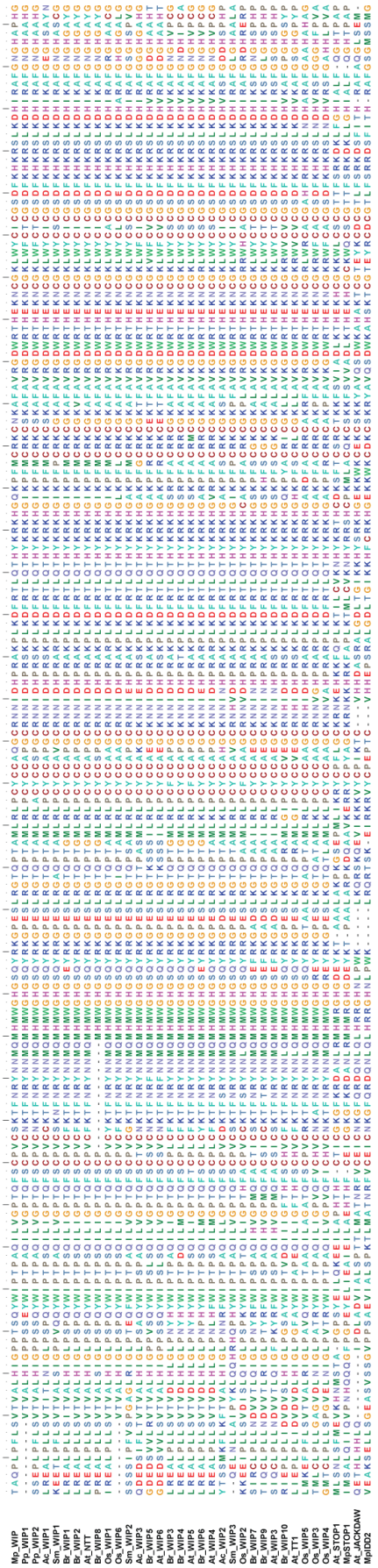

An alignment of the WIP domain of MpWIP and all WIP proteins from *Physcomitrella patens, Selaginella moellendorffii, Oryza sativa, Aquilegia caerulea* and *Arabidopsis thaliana,* and related non-WIP C2H2 zinc finger transcription factors from *M. polymorpha* and *A. thaliana*, AtSENSITIVE TO PROTON RHIZOTOXICITY 1 (AtSTOP1), MpSTOP1, AtJACKDAW (AtJKD) and MpINDETERMINATE(ID)-DOMAIN 2 (MpIDD2). The alignment is provided in FASTA format in Supplementary File 1.

Figure S2

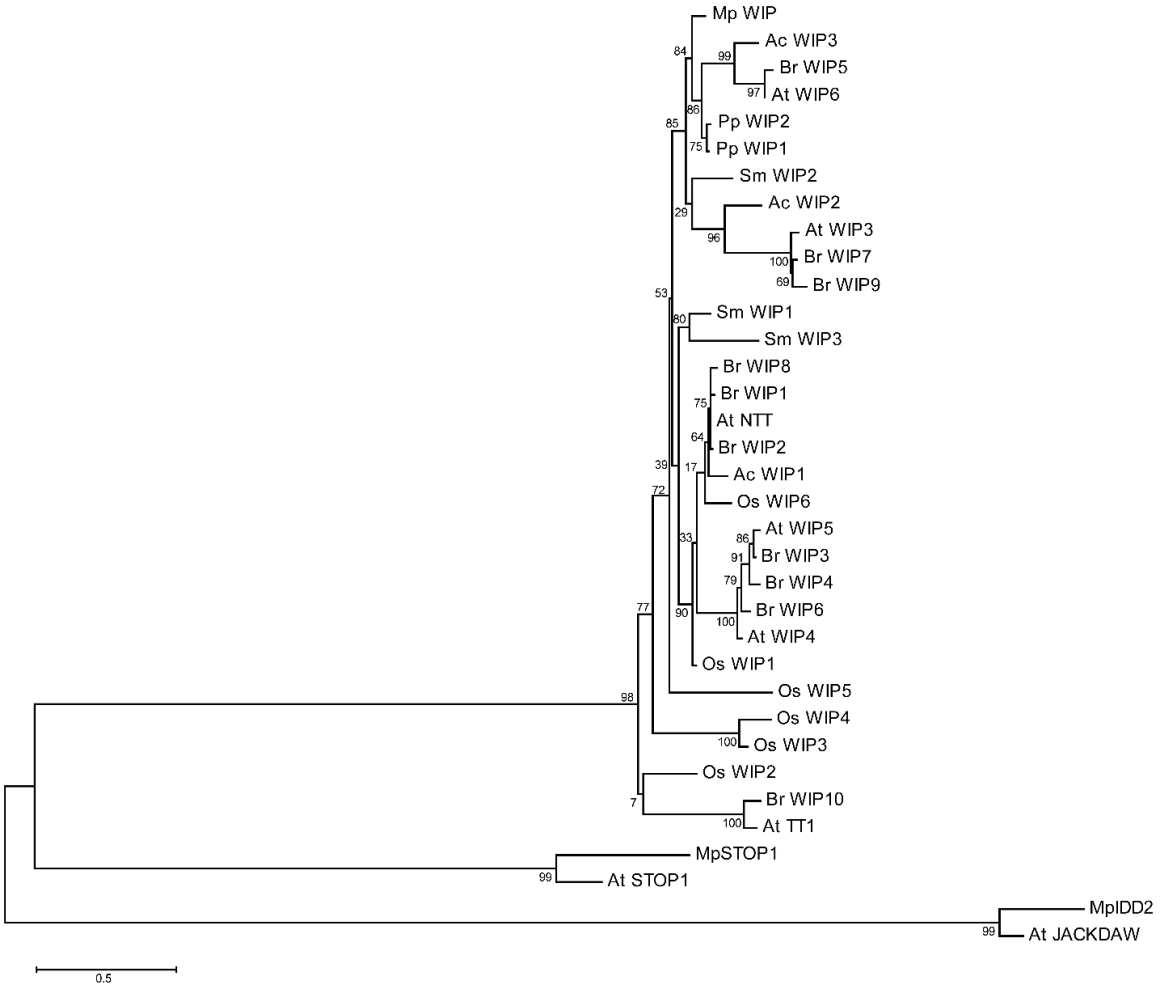

Maximum-likelihood phylogeny of land plant WIP proteins. From the alignment in Figure S1 and Supplemental File 1. Nodes are marked with aLRT values. The *M. polymorpha* protein MpWIP falls into a well-supported clade containing all the WIP proteins from other species (aLRT value = 98).

Figure S3

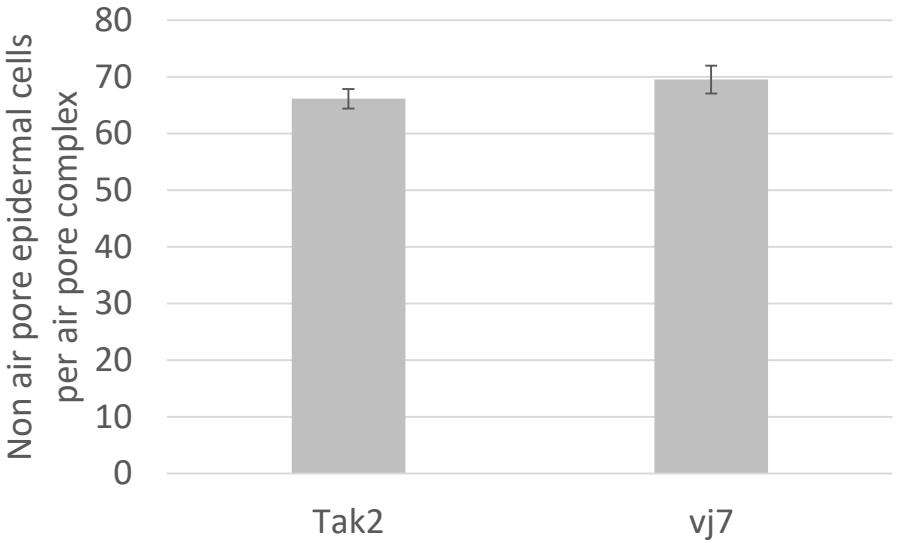

Air pore density in the wild type Tak 2 and the Mp*wip* gain of function mutant *vj7*. Non air pore epidermal cells were counted in 15 mature air chambers for 7 individuals of each genotype. No significant difference in air pore density was observed (Student's T test, p = 0.28). Error bars indicate standard error of the mean.

Figure S4

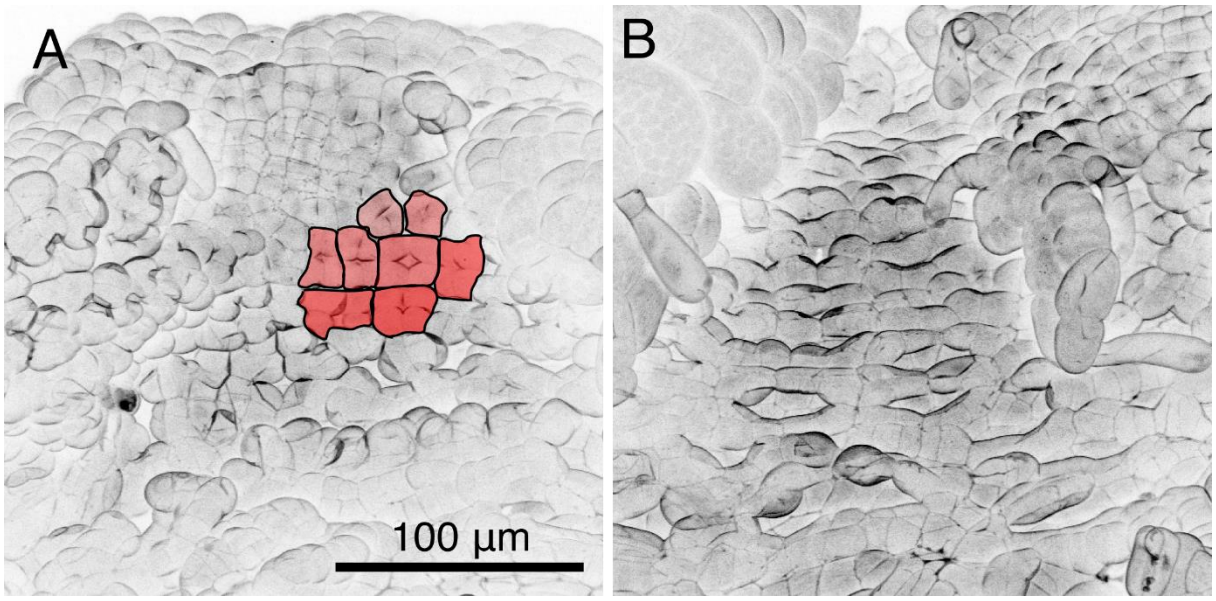

Early stages of air pore complex development in $_{pro}$Os*ACT:amiR*-Mp*WIP-3' UTR*$^{Mp miR160}$. A) As in the wild type, air pore complexes initiate as packets of four epidermal cells (outlined and shaded red). At the point where they meet a schizogenous opening forms. B) The cells surrounding the air pore opening do not divide periclinally, as they do in the wild type. Extra anticlinal divisions occur in these cells, resulting in a single tier of more than four cells. Both panels CSLM, PI stained, 10 d gemmalings, apex at top.

Supplementary Experimental Methods

Plasmid construction

See “List of oligonucleotides used in this study”, below, for sequences of primers.

Constitutive expression of Mp*WIP*

For constitutive expression of Mp*WIP*, Mp*WIP,* including the 3’ and 5’ UTRs, was amplified from wild type genomic DNA using Phusion DNA polymerase with primers MpWIP-F and MpWIP-R and recombined into the pCR8/GW/TOPO Gateway entry vector (Invitrogen). To create the *pro* Os*ACT:*Mp*WIP* expression construct, an LR reaction was carried out between the entry vector and the plasmid *pro*Os*ACT:GATEWAY:TERM*-pMpGW207(Breuninger et al., 2016).

Generation of *pro*Mp*WIP:3xYFP-NLS*

To generate the *pro*Mp*WIP*:*YFP-NLS* expression vector, 4.7 kb of sequence 5’ to the start of the CDS of Mp*WIP* was amplified in 4 overlapping segments using Phusion DNA polymerase with the primer pairs *pro*Mp*WIP*1-F and *pro*Mp*WIP*1-R; *pro*Mp*WIP*2-F and *pro*Mp*WIP*2-R; *pro*Mp*WIP*3-F and *pro*Mp*WIP*3-R; and *pro*Mp*WIP*4-F and *pro*Mp*WIP*4-R. These fragments were joined by overlap PCR using Phusion High-Fidelity DNA Polymerase (New England Biolabs) and primers *pro*Mp*WIP*4-F and *pro*Mp*WIP*1-R, and subcloned into pGEM-T.

The In-Fusion HD Cloning Kit (Clontech Laboratories) was used to introduce this promoter into the binary vector Vp57, based on the plasmid pCambia1300 with the addition of a terminator sequence 3’ to the CaMV 35S promoter that drives expression of the *hpt* gene. The promoter was amplified with the primers *pro*Mp*WIP*InFusion-F and *pro*Mp*WIP*InFusion-R, which add 16 bp of sequence homologous to the desired insertion site on either side, as well as a SacI site at the 3’ terminus of the promoter, and the In-Fusion reaction was performed with Vp57 linearised with SmaI (New England Biolabs). The resulting plasmid was digested with SacI (New England Biolabs), dephosphorylated with Antarctic Phosphatase (New England Biolabs), and the Gateway Vector Conversion System (Thermo Fisher) was used to ligate GW Cassette C.1 in between the promoter and terminator, to generate a destination vector containing *pro*Mp*WIP:GW:Term*. An LR reaction was carried out between this vector and the plasmid “*NLS-3xYFP* in pENTRY3c” (Breuninger et al., 2016) to create an expression vector containing *pro*Mp*WIP:3xYFP-NLS:Term*.

Constitutive expression of MpWIP-SRDX *and* MpWIP-VP16 *fusion proteins*

To generate a fusion between the EAR-motif repression domain (SRDX) and the C-terminus of Mp*WIP,* the Mp*WIP* CDS was amplified from the *pro* Os*ACT:*Mp*WIP* expression vector with Phusion High-Fidelity DNA Polymerase and the primers Mp*WIP*-CDS-F and Mp*WIP*-SRDX-R. Mp*WIP*-SRDX-R replaces the STOP codon of *MpWIP* with sequence encoding the SRDX domain (LDLDLELRLGFA*) (Hiratsu et

al., 2003). This product was recombined into the pCR8/GW/TOPO Gateway entry vector to create the Mp*WIP-SRDX* entry vector.

To generate a fusion between the VP16 activation domain and the C-terminus of Mp*WIP,* the Mp*WIP* CDS was amplified from the $_{pro}$ Os*ACT:*Mp*WIP* expression vector with Phusion High-Fidelity DNA Polymerase and the primers Mp*WIP*-CDS-F and Mp*WIP*-VP16-R. Mp*WIP*-VP16-R replaces the STOP codon of *MpWIP* with sequence encoding the VP16 domain (DALDDFDLEML*) (Seipel et al., 1994). This product was recombined into the pCR8/GW/TOPO Gateway entry vector to create the Mp*WIP-VP16* entry vector.

An LR reaction was carried out between each of these entry vectors and the destination vector "*pro35S:GATEWAY:TERM*-pCAM" (Breuninger et al., 2016).

Mp*WIP artificial microRNA*

The *MpmiR160* pre-miR backbone was used as the basis of amiR design (Flores-Sandoval et al., 2016), with the endogenous *miR160* sequence replaced with 21 nt targeting the Mp*WIP* transcript. miRs were designed using the WMD3 software (http://wmd3.weigelworld.org/) with full-length Mp*WIP* transcript as the target. The highest-ranked *amiRs* targeting the 3' UTR and CDA of *MpWIP,* were chosen. The amiR* was designed to have mismatches with the amiR sequence at positions 7, 13 and 18, following the recommendations of Flores-Sandoval et al., (2016). These were then used to replace the native *miR160* miR and miR* sequences in the backbone. These sequences were each bracketed by attB1 and attB2 sites and synthesised by Life Technologies. These were recombined with pDONR221 using BP Clonase II (Invitrogen) to create entry clones, which were each recombined with plasmid *pro*Os*ACT:GATEWAY:TERM*-pMpGW207 (Breuninger et al., 2016) using LR Clonase II (Thermo Fisher) to generate the expression clones $_{pro}$Os*ACT:amiR*-Mp*WIP-3' UTR*$^{Mp miR160}$ and $_{pro}$Os*ACT:amiR*-Mp*WIP-CDS*$^{Mp miR160}$.

Phylogenetic analysis

The genomic sequence of Mp*WIP* was obtained from an *M. polymorpha* genome prepared from Tak-1 and Tak-2 accessions (Honkanen et al., 2016). This Whole Genome Shotgun project has been deposited at DDBJ/ENA/GenBank under the accession LVLJ00000000. The version described in this paper is version LVLJ01000000. The Mp*WIP* transcript sequence was obtained from an *M. polymorpha* gametophyte transcriptome prepared from Tak-1 and Tak-2 accessions. This Transcriptome Shotgun Assembly project has been deposited at DDBJ/ENA/GenBank under the accession GEFO00000000. The version described in this paper is the first version, GEFO01000000.

To identify homologues in other land plants of the gene linked to the mutant phenotype in mutant *vj7* we used the translation of the longest open reading frame to query the *Arabidopsis* genome using the tblastn algorithm. The most similar match

was At*NO TRANSMITTING TRACT* (At*NTT*) which was 71% identical over the entire length of the protein and a member of the WIP family of zinc finger proteins.

MAFFT v. 7 (Katoh and Standley, 2013) was used to align the sequences of MpWIP and WIP proteins from Physcomitrella patens, Selaginella moellendorffii, Oryza sativa, Aquilegia caerulea and Arabidopsis thaliana, and related non-WIP C2H2 zinc finger transcription factors from M. polymorpha and A. thaliana, AtSENSITIVE TO PROTON RHIZOTOXICITY 1 (AtSTOP1), MpSTOP1, AtJACKDAW (AtJKD) and MpINDETERMINATE(ID)-DOMAIN 2 (MpIDD2), implementing the L-INS-i strategy. The alignment was manually trimmed to remove poorly-aligned regions (Fig. S1, Supplemental File 1). A maximum-likelihood phylogeny was estimated with PhyML 3.0 (Guindon et al., 2010), using the LG substitution model and NNI tree improvement. Branch support was estimated using the aLR-T SH-like method.

Supplementary File 1

Click here to Download Supplementary File 1

List of oligonucleotides used in this study:

Cloning of Mp*WIP*:

Mp*WIP*-F	tctctctctctctctctatc
Mp*WIP*-R	tgtgtcaaacgaatactcgagag

Generation of Mp*WIP* promoter reporter contruct:

*pro*Mp*WIP*1-F	aaatcactgactgcaattgaagg
*pro*Mp*WIP*1-R	acccgaagcttctgaacgta
*pro*Mp*WIP*2-F	cgtgctcagacccccttc
*pro*Mp*WIP*2-R	caccatctgtcatctgagtctgc
*pro*Mp*WIP3*-F	gcccatcataacagcaccac
*pro*Mp*WIP*3-R	ttatttcaagctccgcgacg
*pro*Mp*WIP*4-F	gcagacattgattgaagtcgc
*pro*Mp*WIP*4-R	gggatgatgggcaaggct
*pro*Mp*WIP*InFusion-F	aacgaaagctcgatcctctagacccgaagcttctgaacgtaa
*pro*Mp*WIP*InFusion-R	ttcgagctcggtacccgggttaacgtgctcagacccccttc

Generation of SRDX and VP16 fusions:

Mp*WIP-CDS*-F	atgagctcgaggtaccatgcc
Mp*WIP-SRDX*-R	ctacgcaaagcccaggcgcagttccagatccagatccagttgcgatccggccgac
Mp*WIP-VP16*-R	ctacagcatctccaagtcgaagtcgtccagggcgtcttgcgatccggccgac

RT-PCR:

Mp*WIP*-qRT-F	cgtggggctaatgagaaatg
Mp*WIP*-qRT-R	atgcccatctgaagtcgaag
Mp*ACT*-qRT-F	aggcatctggtatccacgag
Mp*ACT*-qRT-R	acatggtcgttcctccagac
Mp*APT*-qRT-F	cgaaagcccaagaagctacc
Mp*APT*-qRT-R	gtacccccggttgcaataag
Mp*WIP-CDS*-RT-F	ttgcagcaagaccttcaacc
Mp*WIP-SRDX*-RT-R	cagttccagatccagatcca
Mp*WIP-VP16*-RT-R	tccaagtcgaagtcgtcca

SUPPLEMENTARY REFRENCES

Breuninger, H., Thamm, A., Streubel, S., Sakayama, H., Nishiyama, T. and Dolan, L. (2016). Diversification of a bHLH transcription factor family in streptophytes led to the evolution of antagonistically acting genes controlling root hair growth. *Curr. Biol.* **26**, 920–934.

Flores-Sandoval, E., Dierschke, T., Fisher, T. J. and Bowman, J. L. (2016). Efficient and inducible use of artificial microRNAs in *Marchantia polymorpha*. *Plant Cell Physiol.* **57**, 281–90.

Guindon, S., Dufayard, J.-F., Lefort, V. and Anisimova, M. (2010). New alogrithms and methods to estimate maximum-likelihood phylogenies: assessing the performance of PhyML 3.0. *Syst. Biol.* **59**, 307–321.

Hiratsu, K., Matsui, K., Koyama, T. and Ohme-Takagi, M. (2003). Dominant repression of target genes by chimeric repressors that include the EAR motif, a repression domain, in *Arabidopsis*. *Plant J.* **34**, 733–739.

Honkanen, S., Jones, V. A. S., Morieri, G., Champion, C., Hetherington, A. J., Kelly, S., Proust, H., Saint-Marcoux, D., Prescott, H. and Dolan, L. (2016). The mechanism forming the cell surface of tip-growing rooting cells is conserved among land plants. *Curr. Biol.* **26**, 3238–3244.

Katoh, K. and Standley, D. M. (2013). MAFFT multiple sequence alignment software version 7: Improvements in performance and usability. *Mol. Biol. Evol.* **30**, 772–780.

Proust, H., Honkanen, S., Jones, V. A. S., Morieri, G., Prescott, H., Kelly, S., Ishizaki, K., Kohchi, T. and Dolan, L. (2016). *RSL* class I genes controlled the development of epidermal structures in the common ancestor of land plants. *Curr. Biol.* **26**, 93–99.

Seipel, K., Georgiev, O. and Schaffner, W. (1994). A minimal transcription activation domain consisting of a specific array of aspartic acid and leucine residues. *Biol. Chem. Hoppe. Seyler.* **375**, 463–470.

Figure S1

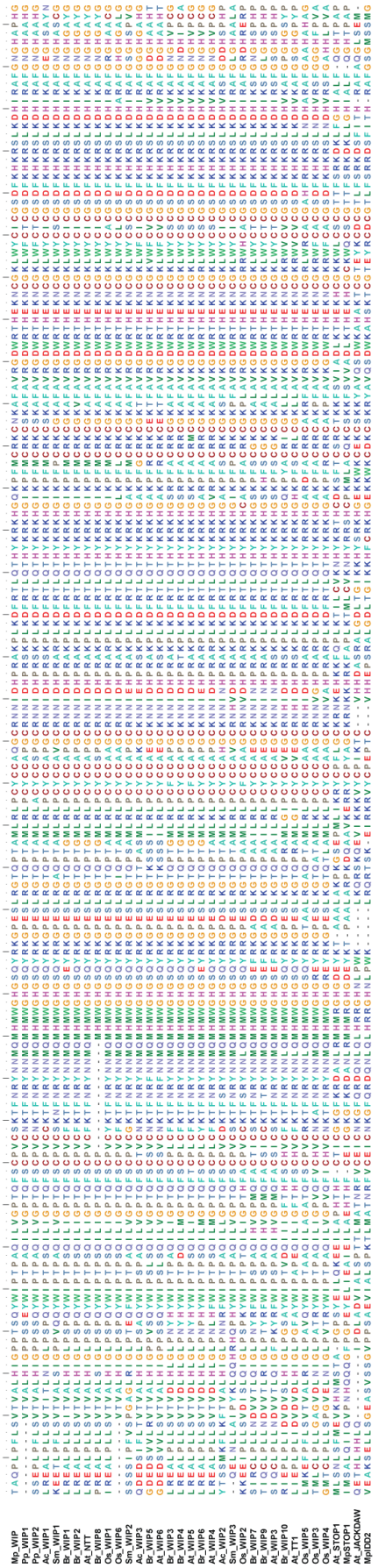

An alignment of the WIP domain of MpWIP and all WIP proteins from *Physcomitrella patens, Selaginella moellendorffii, Oryza sativa, Aquilegia caerulea* and *Arabidopsis thaliana,* and related non-WIP C2H2 zinc finger transcription factors from *M. polymorpha* and *A. thaliana*, AtSENSITIVE TO PROTON RHIZOTOXICITY 1 (AtSTOP1), MpSTOP1, AtJACKDAW (AtJKD) and MpINDETERMINATE(ID)-DOMAIN 2 (MpIDD2). The alignment is provided in FASTA format in Table S2.

Figure S2

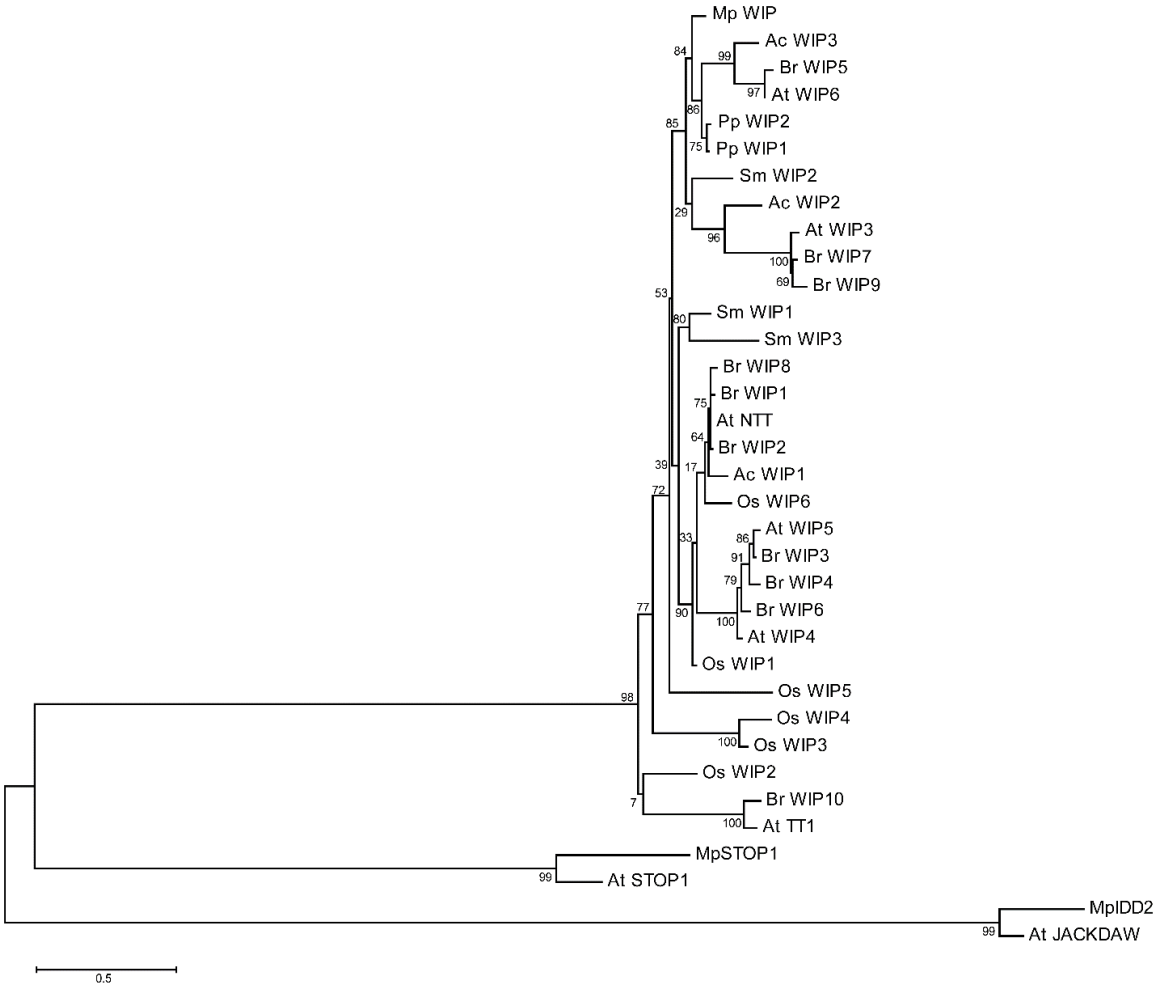

Maximum-likelihood phylogeny of land plant WIP proteins. From the alignment in Figure S1 and Supplemental File 1. Nodes are marked with aLRT values. The *M. polymorpha* protein MpWIP falls into a well-supported clade containing all the WIP proteins from other species (aLRT value = 98).

Figure S3

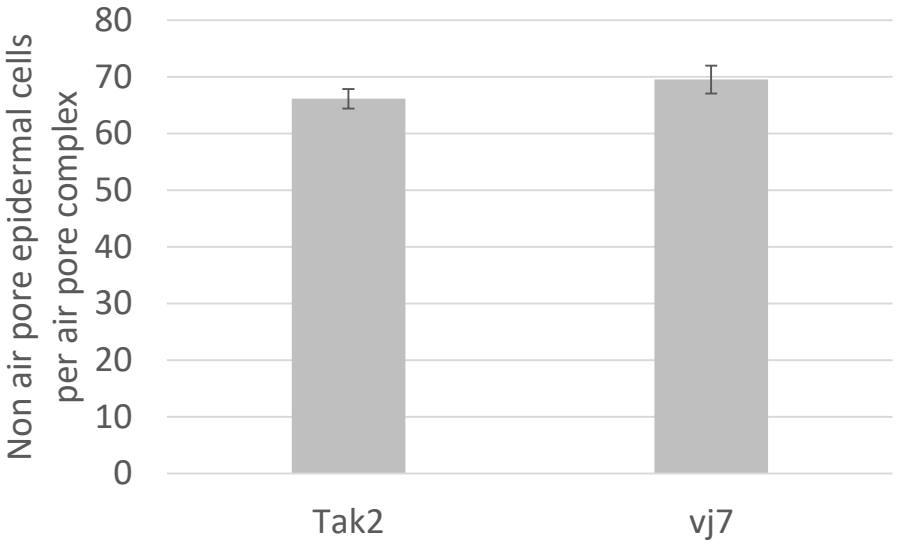

Air pore density in the wild type Tak 2 and the Mp*wip* gain of function mutant *vj7*. Non air pore epidermal cells were counted in 15 mature air chambers for 7 individuals of each genotype. No significant difference in air pore density was observed (Student's T test, p = 0.28). Error bars indicate standard error of the mean.

Figure S4

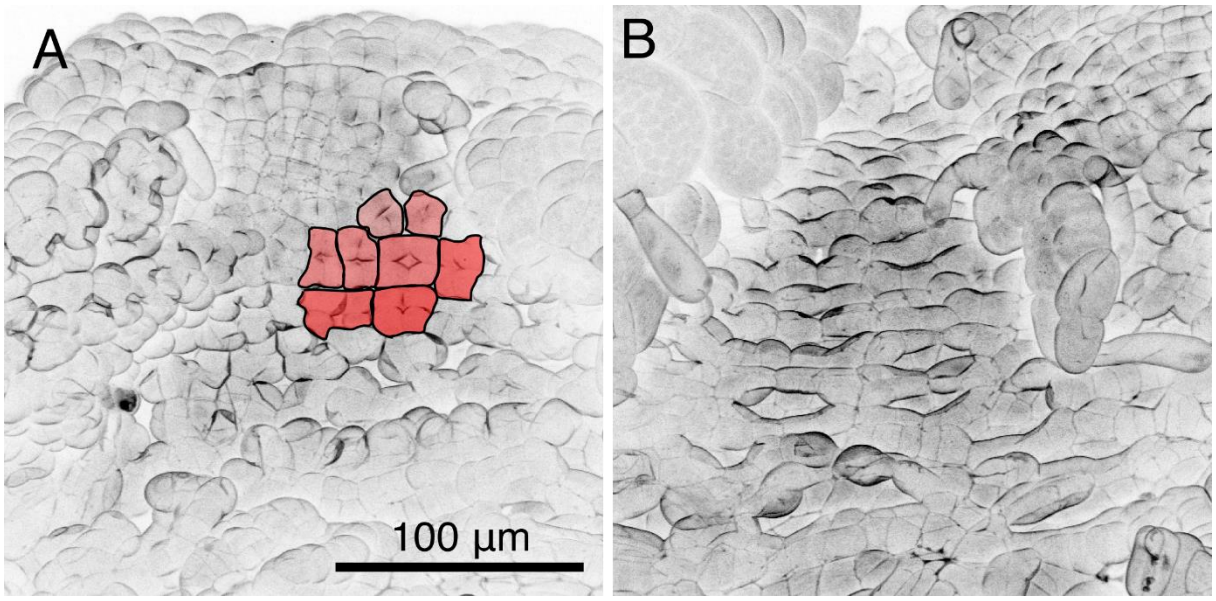

Early stages of air pore complex development in $_{pro}$Os*ACT:amiR*-Mp*WIP-3' UTR*$^{Mp miR160}$. A) As in the wild type, air pore complexes initiate as packets of four epidermal cells (outlined and shaded red). At the point where they meet a schizogenous opening forms. B) The cells surrounding the air pore opening do not divide periclinally, as they do in the wild type. Extra anticlinal divisions occur in these cells, resulting in a single tier of more than four cells. Both panels CSLM, PI stained, 10 d gemmalings, apex at top.

Supplementary Experimental Methods

Plasmid construction

See Table S1 for sequences of primers.

Constitutive expression of Mp*WIP*

For constitutive expression of Mp*WIP*, Mp*WIP,* including the 3' and 5' UTRs, was amplified from wild type genomic DNA using Phusion DNA polymerase with primers MpWIP-F and MpWIP-R and recombined into the pCR8/GW/TOPO Gateway entry vector (Invitrogen). To create the *pro* Os*ACT:*Mp*WIP* expression construct, an LR reaction was carried out between the entry vector and the plasmid *pro*Os*ACT:GATEWAY:TERM*-pMpGW207(Breuninger et al., 2016).

*Generation of pro*Mp*WIP:3xYFP-NLS*

To generate the *pro*Mp*WIP*:*YFP-NLS* expression vector, 4.7 kb of sequence 5' to the start of the CDS of Mp*WIP* was amplified in 4 overlapping segments using Phusion DNA polymerase with the primer pairs *pro*Mp*WIP*1-F and *pro*Mp*WIP*1-R; *pro*Mp*WIP*2-F and *pro*Mp*WIP*2-R; *pro*Mp*WIP*3-F and *pro*Mp*WIP*3-R; and *pro*Mp*WIP*4-F and *pro*Mp*WIP*4-R. These fragments were joined by overlap PCR using Phusion High-Fidelity DNA Polymerase (New England Biolabs) and primers *pro*Mp*WIP*4-F and *pro*Mp*WIP*1-R, and subcloned into pGEM-T.

The In-Fusion HD Cloning Kit (Clontech Laboratories) was used to introduce this promoter into the binary vector Vp57, based on the plasmid pCambia1300 with the addition of a terminator sequence 3' to the CaMV 35S promoter that drives expression of the *hpt* gene. The promoter was amplified with the primers *pro*Mp*WIP*InFusion-F and *pro*Mp*WIP*InFusion-R, which add 16 bp of sequence homologous to the desired insertion site on either side, as well as a SacI site at the 3' terminus of the promoter, and the In-Fusion reaction was performed with Vp57 linearised with SmaI (New England Biolabs). The resulting plasmid was digested with SacI (New England Biolabs), dephosphorylated with Antarctic Phosphatase (New England Biolabs), and the Gateway Vector Conversion System (Thermo Fisher) was used to ligate GW Cassette C.1 in between the promoter and terminator, to generate a destination vector containing *pro*Mp*WIP:GW:Term*. An LR reaction was carried out between this vector and the plasmid "*NLS-3xYFP* in pENTRY3c" (Breuninger et al., 2016) to create an expression vector containing *pro*Mp*WIP:3xYFP-NLS:Term*.

Constitutive expression of MpWIP-SRDX *and* MpWIP-VP16 *fusion proteins*

To generate a fusion between the EAR-motif repression domain (SRDX) and the C-terminus of Mp*WIP,* the Mp*WIP* CDS was amplified from the *pro* Os*ACT:*Mp*WIP* expression vector with Phusion High-Fidelity DNA Polymerase and the primers Mp*WIP*-CDS-F and Mp*WIP*-SRDX-R. Mp*WIP*-SRDX-R replaces the STOP codon of *MpWIP* with sequence encoding the SRDX domain (LDLDLELRLGFA*) (Hiratsu et

al., 2003). This product was recombined into the pCR8/GW/TOPO Gateway entry vector to create the Mp*WIP-SRDX* entry vector.

To generate a fusion between the VP16 activation domain and the C-terminus of Mp*WIP,* the Mp*WIP* CDS was amplified from the $_{pro}$ Os*ACT:*Mp*WIP* expression vector with Phusion High-Fidelity DNA Polymerase and the primers Mp*WIP*-CDS-F and Mp*WIP*-VP16-R. Mp*WIP*-VP16-R replaces the STOP codon of *MpWIP* with sequence encoding the VP16 domain (DALDDFDLEML*) (Seipel et al., 1994). This product was recombined into the pCR8/GW/TOPO Gateway entry vector to create the Mp*WIP-VP16* entry vector.

An LR reaction was carried out between each of these entry vectors and the destination vector "*pro35S:GATEWAY:TERM*-pCAM" (Breuninger et al., 2016).

Mp*WIP artificial microRNA*

The *MpmiR160* pre-miR backbone was used as the basis of amiR design (Flores-Sandoval et al., 2016), with the endogenous *miR160* sequence replaced with 21 nt targeting the Mp*WIP* transcript. miRs were designed using the WMD3 software (http://wmd3.weigelworld.org/) with full-length Mp*WIP* transcript as the target. The highest-ranked *amiRs* targeting the 3' UTR and CDA of *MpWIP,* were chosen. The amiR* was designed to have mismatches with the amiR sequence at positions 7, 13 and 18, following the recommendations of Flores-Sandoval et al., (2016). These were then used to replace the native *miR160* miR and miR* sequences in the backbone. These sequences were each bracketed by attB1 and attB2 sites and synthesised by Life Technologies. These were recombined with pDONR221 using BP Clonase II (Invitrogen) to create entry clones, which were each recombined with plasmid *pro*Os*ACT:GATEWAY:TERM*-pMpGW207 (Breuninger et al., 2016) using LR Clonase II (Thermo Fisher) to generate the expression clones $_{pro}$Os*ACT:amiR*-Mp*WIP-3' UTR*$^{Mp miR160}$ and $_{pro}$Os*ACT:amiR*-Mp*WIP-CDS*$^{Mp miR160}$.

Phylogenetic analysis

The genomic sequence of Mp*WIP* was obtained from an *M. polymorpha* genome prepared from Tak-1 and Tak-2 accessions (Honkanen et al., 2016). This Whole Genome Shotgun project has been deposited at DDBJ/ENA/GenBank under the accession LVLJ00000000. The version described in this paper is version LVLJ01000000. The Mp*WIP* transcript sequence was obtained from an *M. polymorpha* gametophyte transcriptome prepared from Tak-1 and Tak-2 accessions. This Transcriptome Shotgun Assembly project has been deposited at DDBJ/ENA/GenBank under the accession GEFO00000000. The version described in this paper is the first version, GEFO01000000.

To identify homologues in other land plants of the gene linked to the mutant phenotype in mutant *vj7* we used the translation of the longest open reading frame to query the *Arabidopsis* genome using the tblastn algorithm. The most similar match

was At*NO TRANSMITTING TRACT* (At*NTT*) which was 71% identical over the entire length of the protein and a member of the WIP family of zinc finger proteins.

MAFFT v. 7 (Katoh and Standley, 2013) was used to align the sequences of MpWIP and WIP proteins from Physcomitrella patens, Selaginella moellendorffii, Oryza sativa, Aquilegia caerulea and Arabidopsis thaliana, and related non-WIP C2H2 zinc finger transcription factors from M. polymorpha and A. thaliana, AtSENSITIVE TO PROTON RHIZOTOXICITY 1 (AtSTOP1), MpSTOP1, AtJACKDAW (AtJKD) and MpINDETERMINATE(ID)-DOMAIN 2 (MpIDD2), implementing the L-INS-i strategy. The alignment was manually trimmed to remove poorly-aligned regions (Fig. S1, Supplemental File 1). A maximum-likelihood phylogeny was estimated with PhyML 3.0 (Guindon et al., 2010), using the LG substitution model and NNI tree improvement. Branch support was estimated using the aLR-T SH-like method.

Table S1. List of oligonucleotides used in this study:

Cloning of Mp*WIP*:

Mp*WIP*-F	tctctctctctctctctatc
Mp*WIP*-R	tgtgtcaaacgaatactcgagag

Generation of Mp*WIP* promoter reporter contruct:

*pro*Mp*WIP*1-F	aaatcactgactgcaattgaagg
*pro*Mp*WIP*1-R	acccgaagcttctgaacgta
*pro*Mp*WIP*2-F	cgtgctcagacccccttc
*pro*Mp*WIP*2-R	caccatctgtcatctgagtctgc
*pro*Mp*WIP3*-F	gcccatcataacagcaccac
*pro*Mp*WIP*3-R	ttatttcaagctccgcgacg
*pro*Mp*WIP*4-F	gcagacattgattgaagtcgc
*pro*Mp*WIP*4-R	gggatgatgggcaaggct
*pro*Mp*WIP*InFusion-F	aacgaaagctcgatcctctagacccgaagcttctgaacgtaa
*pro*Mp*WIP*InFusion-R	ttcgagctcggtacccgggttaacgtgctcagacccccttc

Generation of SRDX and VP16 fusions:

Mp*WIP-CDS*-F	atgagctcgaggtaccatgcc
Mp*WIP-SRDX*-R	ctacgcaaagcccaggcgcagttccagatccagatccagttgcgatccggccgac
Mp*WIP-VP16*-R	ctacagcatctccaagtcgaagtcgtccagggcgtcttgcgatccggccgac

RT-PCR:

Mp*WIP*-qRT-F	cgtggggctaatgagaaatg
Mp*WIP*-qRT-R	atgcccatctgaagtcgaag
Mp*ACT*-qRT-F	aggcatctggtatccacgag
Mp*ACT*-qRT-R	acatggtcgttcctccagac
Mp*APT*-qRT-F	cgaaagcccaagaagctacc
Mp*APT*-qRT-R	gtacccccggttgcaataag
Mp*WIP-CDS*-RT-F	ttgcagcaagaccttcaacc
Mp*WIP-SRDX*-RT-R	cagttccagatccagatcca
Mp*WIP-VP16*-RT-R	tccaagtcgaagtcgtcca

Table S2. An alignment of the WIP domain of MpWIP and WIP proteins in FASTA format

Click here to Download Table S2

SUPPLEMENTARY REFRENCES

Breuninger, H., Thamm, A., Streubel, S., Sakayama, H., Nishiyama, T. and Dolan, L. (2016). Diversification of a bHLH transcription factor family in streptophytes led to the evolution of antagonistically acting genes controlling root hair growth. *Curr. Biol.* **26**, 920–934.

Flores-Sandoval, E., Dierschke, T., Fisher, T. J. and Bowman, J. L. (2016). Efficient and inducible use of artificial microRNAs in *Marchantia polymorpha*. *Plant Cell Physiol.* **57**, 281–90.

Guindon, S., Dufayard, J.-F., Lefort, V. and Anisimova, M. (2010). New alogrithms and methods to estimate maximum-likelihood phylogenies: assessing the performance of PhyML 3.0. *Syst. Biol.* **59**, 307–321.

Hiratsu, K., Matsui, K., Koyama, T. and Ohme-Takagi, M. (2003). Dominant repression of target genes by chimeric repressors that include the EAR motif, a repression domain, in *Arabidopsis*. *Plant J.* **34**, 733–739.

Honkanen, S., Jones, V. A. S., Morieri, G., Champion, C., Hetherington, A. J., Kelly, S., Proust, H., Saint-Marcoux, D., Prescott, H. and Dolan, L. (2016). The mechanism forming the cell surface of tip-growing rooting cells is conserved among land plants. *Curr. Biol.* **26**, 3238–3244.

Katoh, K. and Standley, D. M. (2013). MAFFT multiple sequence alignment software version 7: Improvements in performance and usability. *Mol. Biol. Evol.* **30**, 772–780.

Proust, H., Honkanen, S., Jones, V. A. S., Morieri, G., Prescott, H., Kelly, S., Ishizaki, K., Kohchi, T. and Dolan, L. (2016). *RSL* class I genes controlled the development of epidermal structures in the common ancestor of land plants. *Curr. Biol.* **26**, 93–99.

Seipel, K., Georgiev, O. and Schaffner, W. (1994). A minimal transcription activation domain consisting of a specific array of aspartic acid and leucine residues. *Biol. Chem. Hoppe. Seyler.* **375**, 463–470.